

# Transient decay from the steady state in the photoconductivity of amorphous semiconductors

H. Cordes,\* G. H. Bauer, and R. Brüggemann†

*Fachbereich Physik, Carl von Ossietzky Universität Oldenburg, D-26111 Oldenburg, Germany*

(Received 10 August 1998)

We introduce a modification to the theory developed by G. J. Adriaenssens, S. D. Baranovskii, W. Fuhs, J. Jansen, and Ö. Öktü [Phys. Rev. B **51**, 9661 (1995)] for the initial decay of the photoconductivity in amorphous semiconductors. With the same physical model and application of the concepts of multiple trapping we derive a theory based upon an emission-rate analysis for the decaying free electron density. We obtain an easy-to-use analytical expression for exponential band tails that links the decay characteristics to the band-tail parameter. A comparison with results from full numerical solutions confirms the validity of our analytical approach and the improvement with respect to the results by Adriaenssens *et al.* We also present solutions, supported by numerical modeling, that relate the power-law exponents for the generation rate dependence of the steady-state photoconductivity with that of the response time for the decay. [S0163-1829(98)06847-7]

## I. INTRODUCTION

In recent publications Adriaenssens, Baranovskii, Fuhs, Jansen, and Öktü<sup>1,2</sup> showed that the well-known standard relations for the measured photoconductivity response time  $\tau_{\text{res}}$  and the steady-state photoconductivity  $\sigma_{\text{ph}}$  in amorphous semiconductors fail to explain the experimentally observed different photogeneration rate dependence of  $\sigma_{\text{ph}}$  and  $\tau_{\text{res}}$ : Assuming an exponential density of states (DOS) distribution in the conduction band tail and applying the standard photoconductivity relations developed by Rose<sup>3</sup> leads to the same expression for the power-law exponent in the generation rate dependencies for the steady-state photoconductivity, defined by  $\sigma_{\text{ph}} \propto G^\gamma$ , and for the response time, given by  $\tau_{\text{res}} \propto G^{-\beta}$ , i.e.,  $\beta = \gamma$ . However, most experiments show generation rate dependencies with  $\beta < \gamma$ . For example, Adriaenssens *et al.* report  $\beta = 0.38$  and  $\gamma = 0.76$  for an amorphous silicon carbide sample, measured at 200 K.

The puzzle of the experimental  $\beta \neq \gamma$  results was tackled to be solved by Adriaenssens *et al.* for low illumination intensities by developing a theory on the basis of multiple trapping that accounts for the initial decay of the photocurrent and predicts a stretched exponential decay. Numerical modeling, however, which showed deviations with the results of this analytic approach, motivated us to introduce a modification of their theory, which results in good agreement with the numerical modeling. With both the analytic approach and the simulation as a base we shall derive the relationship between  $\gamma$  and  $\beta$ , which will be seen to depend also on the value of the generation rate. We note here that the relation  $\gamma = 1/(1 + kT/kT_0)$  from the Rose analysis for steady state photoconductivity<sup>3</sup> that links  $\gamma$  with the tail parameter  $kT_0$  of an exponential band tail is a precondition for the above-mentioned equality  $\beta = \gamma$  to hold.

## II. THEORY AND NUMERICAL MODELING

### A. Physical and mathematical model

We employ the same physical model for the amorphous semiconductor as outlined in Ref. 1. It consists of a conduction bandtail with an exponentially decreasing density of states

$$g(E) = g(E_c) \exp(-E/kT_0), \quad (1)$$

where  $g(E_c)$  is the density of states at the band edge  $E_c$  and  $kT_0$  is the tail parameter. Note that we take the energy to be zero at the conduction-band edge and increasing towards midgap. Conduction is considered by the free carriers at  $E_c$  only, which interact with the band tail via capture and release and the effective density of conduction-band states is  $g(E_c)kT$ . Recombination is included by a time-independent free-carrier recombination lifetime  $\tau_0$ . We neglect all carrier transitions between localized states and the valence band. Thus the photocurrent response is governed by the following rate equations for the free-electron density  $n$ :

$$\begin{aligned} \frac{dn(t)}{dt} = & -\frac{n(t)}{\tau_0} - C_n n(t) \int_0^\infty [g(E) - n_t(E)] dE \\ & + \int_0^\infty \nu(E) n_t(E) dE, \end{aligned} \quad (2)$$

and for the localized electron density  $n_t$  at each energy

$$\frac{dn_t(E)}{dt} = -\nu(E) n_t(E) + C_n n(t) [g(E) - n_t(E)]. \quad (3)$$

In this model the principle of detailed balance requires the release rate  $\nu(E)$  to depend exponentially on energy  $\nu(E) = \nu_0 \exp(-E/kT)$ , where the attempt to escape frequency  $\nu_0$  is related to the capture coefficient  $C_n$  via  $\nu_0 = g(E_c)kTC_n$ .

We applied a numerical program, developed on the basis of the LSODI package<sup>4</sup> for ordinary differential equations, to solve the system of equations for the numerical calculation of  $n(t)$  and the energetic distribution of the trapped carrier density.

### B. Analytical approximation: review

We guide the reader through the theory by Adriaenssens *et al.* and introduce some variables that will be needed in the later part of this paper. The theory is based on the case of the multiple trapping model put forward by Tiedje and Rose and

others,<sup>5-7</sup> which is often referred to as the TROK model. In this model a demarcation energy  $\epsilon(t) = kT \ln(\nu_0 t)$  separates those states that are in quasithermal equilibrium with the conduction band due to repeated emitting and retrapping from those states that are too deep for a trapped electron to be emitted yet. Applied to the case after termination of steady-state illumination the trapped electrons above  $\epsilon(t)$  are distributed according to the Boltzmann function in alignment with the free electron density  $n(t)$ , while the electron density below  $\epsilon(t)$  has not changed yet. They therefore follow a Boltzmann distribution that aligns with the initial free-electron density  $n_0 = G\tau_0$ , established in the steady-state, where  $G$  is the steady-state photogeneration rate.

The probability for a free electron to recombine is  $1/\tau_0$ , while its probability  $1/\tau_c$  to be trapped in the band tail is proportional to the density of free states in the tail with

$$1/\tau_c = C_n \int_0^\infty [g(E) - n_t(E)] dE \approx C_n \int_0^\infty g(E) dE. \quad (4)$$

Therefore the probability for a free electron to be recaptured to a localized state rather than to recombine,  $W_c$ , is

$$W_c = \frac{1/\tau_c}{1/\tau_c + 1/\tau_0} = \frac{1}{1 + \tau_c/\tau_0}. \quad (5)$$

Now the aim is to get an expression for the free-electron density at a given time  $t$  after the switch off. We first introduce by  $N_{\text{MT}}[t', \epsilon(t)]$  the density of electrons that are trapped above  $\epsilon(t)$  at a certain time  $t'$  smaller than  $t$ . In our notation  $N_{\text{MT}}[t_0, \epsilon(t)]$  with  $t_0 = 0$  s is the density of electrons, that are trapped above  $\epsilon(t)$  in the steady state before the switch off. We further introduce by  $m(t')$  the average number that an electron out of  $N_{\text{MT}}[t_0, \epsilon(t)]$  will have appeared at the mobility edge until time  $t'$  after switching off the photogeneration. Then until time  $t' = t$  the density of electrons above  $\epsilon(t)$  will have decreased to

$$N_{\text{MT}}[t, \epsilon(t)] = N_{\text{MT}}[t_0, \epsilon(t)] \times W_c^{m(t)}. \quad (6)$$

As previously noted in the TROK model the electron distributions above  $\epsilon(t)$  at  $t_0$  and at  $t$  are approximated by the corresponding Boltzmann functions. Thus their total densities are

$$\begin{aligned} N_{\text{MT}}[t_0, \epsilon(t)] &\approx \int_0^{\epsilon(t)} g(E) \frac{n_0}{N_c} e^{E/kT} dE \\ &= \frac{g(E_c)kT}{N_c} \frac{1}{(1-\alpha)} n_0 [(\nu_0 t_0)^{1-\alpha} - 1] \end{aligned} \quad (7)$$

and

$$\begin{aligned} N_{\text{MT}}[t, \epsilon(t)] &\approx \int_0^{\epsilon(t)} g(E) \frac{n(t)}{N_c} e^{E/kT} dE \\ &= \frac{g(E_c)kT}{N_c} \frac{1}{(1-\alpha)} n(t) [(\nu_0 t)^{1-\alpha} - 1], \end{aligned} \quad (8)$$

where  $\alpha = kT/kT_0$ . Combining these two equations with Eq. (6) leads to

$$n(t) = n_0 W_c^{m(t)} = n_0 \exp(-m(t) |\ln W_c|), \quad (9)$$

which is the expression given in Ref. 1. We note that these expressions are only valid  $\epsilon(t) < E_{\text{fn}}$ , where  $E_{\text{fn}}$  is the quasi-Fermi-energy, measured from  $E_c$ . For the expression for  $m(t)$  Adriaenssens *et al.* assume that an electron will be trapped and reemitted to the conduction band until it is trapped below  $\epsilon(t)$ , from which it will not be reemitted before time  $t$ . The probability  $W_\epsilon(t)$  for an electron to be trapped below  $\epsilon(t)$  rather than above is just the ratio of states

$$W_\epsilon(t) = \int_{\epsilon(t)}^\infty g(E) dE \Big/ \int_0^{\infty} g(E) dE. \quad (10)$$

Therefore a typical electron has to appear at the mobility edge on average  $m(t) = W_\epsilon(t)^{-1} = (\nu_0 t)^\alpha$  times before being trapped below  $\epsilon(t)$ . Using  $m(t)$  in Eq. (9) Adriaenssens *et al.* come to the conclusion that the photocurrent will decay like

$$n(t) = n_0 \exp\left(-(\nu_0 t)^\alpha \left| \ln \frac{1}{1 + \tau_c/\tau_0} \right| \right). \quad (11)$$

### C. Analytical approximation: modification

Based on the rate equations, (2) and (3) tracking the capture and emission rates we derive a different expression than Adriaenssens *et al.* for the typical number  $m(t)$  that an electron will appear at  $E_c$  before recombination until time  $t$ .

Consider again all trapped electrons above a given energy  $\epsilon(t) \leq E_{\text{fn}}$ . In the TROK model the total release rate of trapped electrons at the time  $t'$ ,  $R_r$  is

$$R_r(t') = \int_0^{\epsilon(t')} \nu(E) n_t(E, t') dE. \quad (12)$$

As introduced by Adriaenssens *et al.*,  $W_c$  is the fraction of the released electrons that will be retrapped, leaving  $1 - W_c$  to be the fraction that recombines. Thus the total change per unit time of  $N_{\text{MT}}[t', \epsilon(t)]$  is approximately the release rate multiplied by  $W_c - 1$ ,

$$\frac{d}{dt'} N_{\text{MT}}[t', \epsilon(t)] \approx \int_0^{\epsilon(t')} \nu(E) n_t(E, t') dE \times (W_c - 1). \quad (13)$$

This equation can readily be solved to

$$N_{\text{MT}}[t', \epsilon(t)] \approx N_{\text{MT}}[t_0, \epsilon(t)] \exp[m(t')(W_c - 1)], \quad (14)$$

with

$$m(t') = \int_0^{t'} \frac{\int_0^{\epsilon(t'')} \nu(E) n_t(E, t'') dE}{\int_0^{\epsilon(t')} n_t(E, t') dE} dt''. \quad (15)$$

In our approach  $m(t')$  is the average number of emission and thus trapping events until time  $t'$ , calculated from the time-dependent release rate  $R_r$  in the denominator divided by the time-dependent density of trapped electrons between  $E_c$  and the demarcation energy  $\epsilon(t)$ ,  $N_{\text{MT}}[t'', \epsilon(t)]$ .

Now we are only interested in  $N_{\text{MT}}[t, \epsilon(t)]$ , that is the trapped electron density above  $\epsilon(t)$  at time  $t' = t$  because it is not until time  $t$  that the electrons above  $\epsilon(t)$  follow the Boltzmann distribution and we can use Eq. (8) to relate  $N_{\text{MT}}$  to  $n(t)$ . Setting  $t' = t$ , Eqs. (14) and (15) become

$$N_{\text{MT}}[t, \epsilon(t)] \approx N_{\text{MT}}[t_0, \epsilon(t)] \exp[m(t)(W_c - 1)] \quad (16)$$

and

$$m(t) = \int_0^t \frac{\int_0^{\epsilon(t'')} \nu(E) n_t(E, t'') dE}{\int_0^{\epsilon(t'')} n_t(E, t'') dE} dt'' \quad (17)$$

Note that since  $W_c$  is close to unity, Eq. (16) equals Eq. (6), as can be seen by  $W_c^m = \exp[m \ln(W_c)] \approx \exp[m(W_c - 1)]$ . Combining Eq. (16) with Eqs. (7) and (8) leads to a similar expression for the free-electron density development,

$$n(t) = n_0 \exp[-m(t)(1 - W_c)], \quad (18)$$

as was found by Adriaenssens *et al.*, with the important distinction that we have a different definition for  $m(t)$ .

Approximating the trapped electron distributions in Eq. (17) by the corresponding Boltzmann function, that is, applying the TROK model, leads to

$$\begin{aligned} m(t) &\approx \int_0^t \frac{\int_0^{\epsilon(t')} \nu_0 e^{-E/kT} g(E_c) e^{-E/kT_0} [n(t')/N_c] e^{E/kT} dE}{\int_0^{\epsilon(t')} g(E_c) e^{-E/kT_0} \left[ \frac{n(t')}{N_c} \right] e^{E/kT} dE + \int_{\epsilon(t')}^{\epsilon(t)} g(E_c) e^{-E/kT_0} [n_0/N_c] e^{E/kT} dE} dt' \\ &= \int_0^t \frac{-\nu_0 k T_0 [(\nu_0 t')^{-\alpha} - 1] n(t')}{\left( \frac{kT}{1-\alpha} \right) [(\nu_0 t)^{1-\alpha} n_0 - (\nu_0 t')^{1-\alpha} [n_0 - n(t')] - n(t')]} dt'. \end{aligned} \quad (19)$$

Unfortunately Eq. (18) with this expression for  $m(t)$  cannot be solved analytically to obtain  $n(t)$ . However, if we substitute the actual density  $n(t')$  by the initial free-electron density  $n_0$  in Eq. (19), which is a good approximation at short times, we can solve Eq. (18) analytically. First we get

$$m(t) \approx \int_0^t \frac{-\nu_0 k T_0 [(\nu_0 t')^{-\alpha} - 1]}{\left( \frac{kT}{1-\alpha} \right) [(\nu_0 t)^{1-\alpha} - 1]} dt', \quad (20)$$

where we can neglect  $(\nu_0 t')^{-\alpha}$  in the numerator, because it becomes small compared to 1 as soon as  $t' > \nu_0^{-1}$ . For  $\alpha < 1$ , we also can neglect the 1 compared to  $(\nu_0 t')^{1-\alpha}$  in the denominator leading to

$$m_a \approx \left( \frac{1}{\alpha} - 1 \right) (\nu_0 t)^\alpha \quad \text{if } \alpha < 1, \quad (21)$$

where the index  $a$  indicates that we get an analytical solution for  $n(t)$  with this expression for  $m(t)$ . In the opposite case of  $\alpha > 1$  we can neglect  $(\nu_0 t')^{1-\alpha}$  compared to 1 in the denominator to get

$$m_a \approx \left( 1 - \frac{1}{\alpha} \right) \nu_0 t \quad \text{if } \alpha > 1. \quad (22)$$

The analytical expressions for  $n(t)$  with  $m_a$  are thus

$$n(t) \approx n_0 \exp \left[ - \left( \frac{1}{\alpha} - 1 \right) (\nu_0 t)^\alpha \frac{1}{1 + \tau_0 / \tau_c} \right], \quad \text{if } \alpha < 1, \quad (23)$$

and

$$n(t) \approx n_0 \exp \left[ - \left( 1 - \frac{1}{\alpha} \right) \nu_0 t \frac{1}{1 + \tau_0 / \tau_c} \right], \quad \text{if } \alpha > 1. \quad (24)$$

Alternatively, we also apply Eq. (18) by solving

$$n(t) - n_0 \exp[-m(t)(1 - W_c)] = 0 \quad (25)$$

for  $n(t)$ , where  $m(t)$  is defined as in Eq. (19) and contains the whole development of  $n$  until the inspected time  $t$ , including  $n(t)$  itself. In this seminumerical approach we rely on our analytical expression for  $n(t)$  but solve Eq. (25) numerically for its root, using the previously calculated free-electron decay  $n(t')$  with  $t' < t$ . For these solutions we shall use  $m_n(t)$ , where the index  $n$  denotes the numerical treatment for the analytical expressions.

The response time  $\tau_{\text{res}}$  of the photoconductivity decay can be predicted by calculating the time at which  $n(t)$  after Eq. (23) has fallen to  $1/e$  of its initial value, yielding

$$\tau_{\text{res}} \approx \nu_0^{-1} \left( \frac{\nu_0 \tau_0}{1-\alpha} \right)^{1/\alpha}, \quad (26)$$

where we used the relation  $\tau_c^{-1} = \nu_0 / \alpha$ . Thus the response time varies with the generation rate like  $\tau_{\text{res}} \propto G^{-\beta}$  with

$$\beta = \frac{1-\gamma}{\alpha}, \quad (27)$$

the same dependence as achieved in Ref. 1.

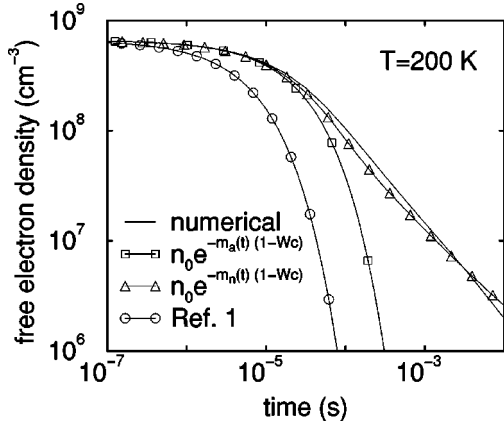


FIG. 1. Transient decay of the free electron density calculated by numerical modeling (full line) and after our two formulas (lines with symbols), together with the formula of Adriaenssens *et al.* (Ref. 1). Results are for  $T=200$  K and  $\alpha=0.73$ .

### III. RESULTS

#### A. Transient decay

Figure 1 compares the calculated free electron decays at  $T=200$  K and with  $kT_0=23.6$  meV,  $C_n=1.45\times 10^{-8}$  cm<sup>3</sup> s<sup>-1</sup> and  $\tau_0=6.6\times 10^{-8}$  s. These values correspond to the fit parameters given by Adriaenssens *et al.* assuming that  $g(E_c)=4\times 10^{21}$  cm<sup>-3</sup> eV<sup>-1</sup>. The photogeneration rate before the switch off was  $G=10^{16}$  cm<sup>-3</sup> s<sup>-1</sup>.

The solid line represents the solution of the discretized rate equations (2) and (3) obtained numerically with the application of the LSODI package. The square-labeled curve represents the decay calculated by  $n(t)=n_0\exp[-m_a(t)(1-W_c)]$ , where  $m_a(t)$  is defined as in Eq. (21) at  $T=200$  K. It matches with the full numerical solution during the initial decay, that is as long as  $n(t)/n_0$  is not too small.

Salient agreement with the full numerical solution is achieved by solving our analytical expression  $n(t)=n_0\exp[-m_n(t)(1-W_c)]$ , where  $m_n(t)$  is defined as in Eq. (19), numerically.

In comparison, the analytically calculated free electron decay by the formula of Adriaenssens *et al.* given by Eq. (11) falls off too quickly.

For the parameter set of Figs. 1 and 2 the calculated energetic distribution of the trapped electron density and its thermalization behavior at  $T=200$  K is shown. Note the logarithmic scale of the top abscissa, which illustrates the drop in the free-electron density within a few microseconds when  $\epsilon(t)$ , schematically shown by the dashed lines, is still far away from  $E_{fn}$ . The thick lines mark the electron density distributions in the steady state before the switch off ( $t=0$  s) and at  $t=0.1$  ms after the switch off. The approximated density distribution used in the TROK model is schematically shown for  $t=0.1$  ms by the dashed lines that exhibit a step-like shape that follows the numerically calculated trapped electron distribution. In comparison to the thermalization after a light pulse it can be seen that  $\epsilon(t)$  is not related to the maximum of the trapped carrier distribution, which remains at a few times  $10^{13}$  cm<sup>-3</sup> eV<sup>-1</sup> until  $\epsilon(t)$  has reached  $E_{fn}$ , at a time at which  $n$  and thus the photocurrent has dropped to a

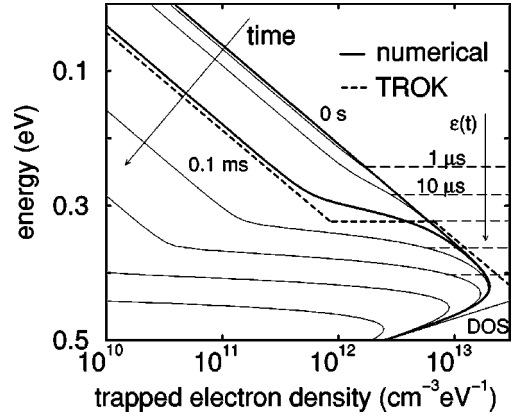


FIG. 2. Time-dependent energetic distributions of the trapped electron density, calculated by numerical modeling and the approximate distribution at  $t=0.1$  ms used in the TROK model. The demarcation energy is also depicted.

significant degree. In contrast, our simulations show that in the high- $G$  regime (see below) the maximum of  $n_t$  thermalizes together with  $\epsilon(t)$ .

Good agreement with our analytical approach is also found, if parameter values are changed. Figure 3 represents the calculated electron decays for  $\tau_0=10^{-10}$  s and  $G=10^{19}$  cm<sup>-3</sup> s<sup>-1</sup>. While the decay after Ref. 1 is too fast, our solutions with  $m_n(t)$  and  $m_a(t)$  represent a good fit to the numerically calculated decay.

Figure 4 shows the simulated electron decay for the case of  $\alpha>1$  with all the parameters as in Fig. 1 but at  $T=300$  K. Our two approaches, calculated after Eq. (25), and the analytical solution calculated with Eq. (24) show good agreement with the numerical results.

#### B. Relation between $\gamma$ and $\beta$

The photogeneration rate dependence of the numerically calculated response times  $\tau_{res}$ , which is defined in Fig. 5 as  $\tau_{1/e}$  by the time when the free-electron density has decayed to  $n_0/e$ , is shown for the same parameters as in Fig. 1. Here we assumed the free-electron recombination lifetime  $\tau_0$  from  $G=n/\tau_0$  to vary with the photogeneration rate like

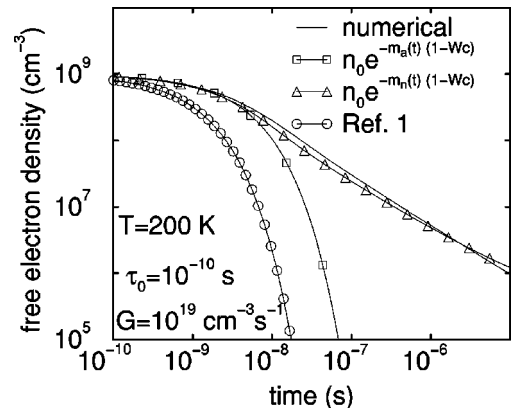


FIG. 3. The full numerical solution in comparison with our analytical and seminumerical approach: transient electron density decay for the same parameters as in Fig. 1 but with  $\tau_0=10^{-10}$  s and  $G=10^{19}$  cm<sup>-3</sup> s<sup>-1</sup>.

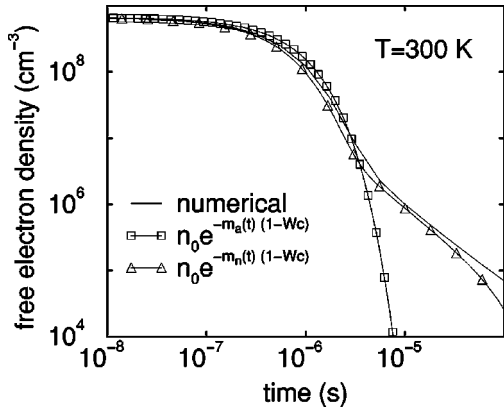


FIG. 4. Good agreement with the full numerical solution for our analytical [with  $m_a(t)$ ] and seminumerical approach [with  $m_n(t)$ ]: transient electron density decay at  $T=300$  K and  $\alpha=1.1$ .

$$\tau_0 \propto G^{\gamma-1}, \quad (28)$$

which is often found experimentally. In Fig. 5 we calculated the response times from the simulated decay curves for different values of  $\gamma$  from  $\gamma=1$  to  $\gamma=0.8$  to  $\gamma$  from the Rose analysis with

$$\gamma = \frac{1}{1+\alpha}, \quad (29)$$

that is,  $\gamma \approx 0.58$  for  $\alpha=0.73$ .

In the latter case the evaluation of the generation rate dependence of the response time  $\tau_{\text{res}}$  from Fig. 5 results in a power law  $\tau_{\text{res}} \propto G^{-\beta}$  with a constant  $\beta$  for all generation rates yielding  $\beta \approx \gamma = 0.58$ .

For the higher values of  $\gamma$  like 0.8 and 1 in Fig. 5, taking  $\gamma \neq 1/1+\alpha$ , we find two different regimes for the  $G$  dependence. The proportionality of  $\tau_{\text{res}}$  changes from a power law  $\tau_{\text{res}} \propto G^{-\beta_1}$  at low  $G$  to  $\tau_{\text{res}} \propto G^{-\beta_2}$  at high  $G$  with  $\beta_1 < \beta_2 < \gamma$ .

It is interesting to see that at high  $G$  the Rose analysis with the popular relation  $\tau_{\text{res}} \approx (1+N_t/n)\tau_0$  results in the same  $G$  dependence as obtained from the numerical analysis although the absolute value is slightly different. An inspection of the time dependence of the decays shows that these

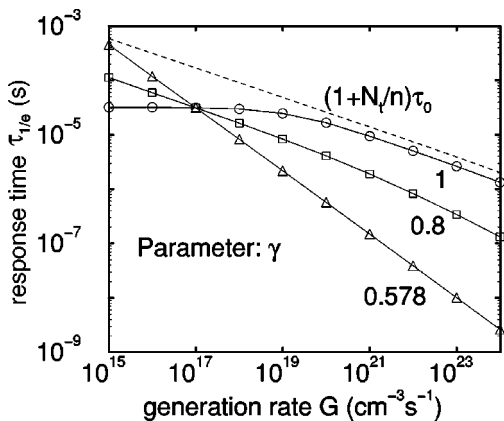


FIG. 5. Generation rate dependence of the response time, given here by the time  $\tau_{1/e}$ , for different values of  $\gamma$ . The results for  $\tau_{1/e} = (1+N_t/n)\tau_0$  are only shown for the case  $\gamma=1$  (dashed line). The evaluation of the slopes is summarized in Table I.

TABLE I. Summary of the evaluation for  $\beta$  from the numerical simulation of the electron decay in Fig. 5 where a low and a high- $G$  regime can be identified. The right two columns contain the values from the analytic theories as discussed in the text and can be compared with the numerical value for  $\beta$ .

$\gamma$	$G$ regime	$\beta$ (Fig. 5)	$(1-\gamma)/\alpha$	$1-\alpha\gamma$
1	low	0.001	0	
1	high	0.283		0.27
0.8	low	0.276	0.274	
0.8	high	0.385		0.378
0.578	low	0.579	0.578	
0.578	high	0.587		0.578

are nonexponential in time and follow a power law but that the exponential behavior from the Rose analysis according to  $n(t) \propto \exp(-t/\tau_{\text{res}})$  is a good approximation at short times for determining  $\tau_{\text{res}}$ . In contrast, at lower  $G$ ,  $\tau_{\text{res}}$  from the Rose analysis is no longer valid as can be seen from the large difference compared to the decay times determined numerically and from our approach, which become much smaller.

The evaluation results from the simulation for  $\beta$  in Table I represent low- and high- $G$  regimes for  $\beta$ : At low  $G$ ,  $\beta$  follows  $\beta = (1-\gamma)/\alpha$  as derived with the analytical model in Sec. II C whereas at high  $G$  the result is  $\beta = 1-\alpha\gamma$ .

#### IV. DISCUSSION

We would like to point out that our discussion on the time dependence and  $G$  dependence is related to the initial decay after termination of the photogeneration. We thus concentrate on the initial time range in which mainly the majority carrier properties determine the photoresponse. At longer times the minority carriers may also become important,<sup>8</sup> which can only be dealt with within a more sophisticated physical model.

##### A. Time dependence

We introduced different formulas for calculating the decay of the electron density that only differ by the way  $m(t)$  is defined, where  $m(t)$  stands for the typical number an electron will have appeared at the conduction band until time  $t$ . These results can be compared with the full numerical solutions that give the correct mathematical solution of the discussed model in order to increase the confidence into the validity of the approximations.

Our analytical approach with the results for the decays for  $\alpha < 1$  result in a significant improvement compared to Ref. 1 for the analytical description of the electron decay after termination of steady-state illumination. The tests in comparison with the numerical solutions in Figs. 1 and 3 show good agreement with the use of  $m_a$  on a short time scale for the initial decay. This time range is usually accessed in the experiment. That for longer times the  $m_a$ -decay behavior deviates from the numerical solution is easily understood due to the replacement of  $n(t)$  by  $n_0$  made in the derivation of  $m_a(t)$ . This approximation becomes more and more crude as the free electron density decays. Using the seminumerical approach of Eq. (25) results in good agreement also for longer times.

Figure 4 illustrates that our approach is not only valid for  $\alpha < 1$  but also for  $\alpha > 1$  with Eq. (24). The latter case is of importance experimentally as amorphous semiconductors such as hydrogenated amorphous silicon with its steep conduction band tail have  $\alpha$  values larger than unity for higher temperatures.

The salient agreement, obtained by using seminumerical approach with  $m_n(t)$ , shows that the TROK model is a well applicable approximation to the large-signal photocurrent decay from the steady state. We have detailed the energetic distributions of the trapped electron density during the decay in Fig. 2 in comparison with the simplified TROK expressions. These results show the steplike shape for the trapped electron distributions: The density of trapped electrons below  $\epsilon(t)$  is unaffected, between  $\epsilon(t)$  and  $E_c$  the quasithermal distribution as expected from TROK is established.

No good agreement is achieved by using the formula developed by Adriaenssens *et al.* in comparison with the numerical solution. Their definition for  $m(t)$  differs from our Eq. (21) just by the factor  $1/\alpha - 1$  leading to too early a decay if  $\alpha = kT/kT_0 > 0.5$ , and to too slow a decay if  $\alpha < 0.5$ . As described in Sec. II B, they assume that an electron will be trapped and reemitted to the conduction band until it is trapped below  $\epsilon(t)$ , from which it will not be reemitted before time  $t$ . Since no transition from localized states to defects or the valence band is included in the model, the trapped electron density below  $\epsilon(t)$  should increase after the switch off according to this reasoning. This is not supported by our numerical modeling as can be seen in Fig. 2 and cannot be the case by the following argument: In the steady state before the switch off those deep traps were in dynamical quasiequilibrium with the conduction band. That is, the trapping rate of free electrons into the localized states equals their emission rate. After termination of the illumination the free electron density  $n$  decreases and so does the trapping rate, while the emission rate remains nearly constant. Thus we expect a small decrease of the trapped electron density instead of the increase resulting from the approach in Ref. 1.

### B. Generation-rate dependence

Comparison between the analytical values of our approach with the numerically calculated response times, Fig. 5, shows excellent agreement at low  $G$ , whereas at high generation rates  $\beta$  is well fitted by the Rose relation

$$\beta = 1 - \alpha\gamma, \quad (30)$$

resulting from  $\tau_{\text{res}} = (1 + N_t/n)\tau_0$ , where  $N_t$  is the density of trapped electrons. This change in  $\beta$  occurs because at high generation rates the demarcation energy  $\epsilon(t)$  reaches the quasi-Fermi-level before the free-electron density has decayed to  $(1/e)n_0$ .

Figure 6 illustrates the trapped electron distribution for such a case. During the initial decay the free-electron density tracks with the maximum of  $n_t$  and approximately with  $N_t$ . Thus in the high generation rate regime our theory is not valid for the response time and the Rose analysis should be applied to calculate  $\tau_{\text{res}}$ .

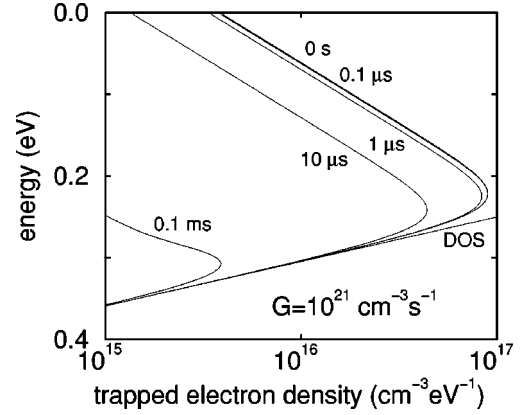


FIG. 6. Time-dependent energetic distributions of the trapped electron density for high  $G$  at  $10^{21} \text{ cm}^{-3} \text{ s}^{-1}$ , calculated by numerical modeling.

It can be shown<sup>9,10</sup> that analytically  $n(t)$  decays with a superposition of being  $\propto t^{1/(1-\alpha)}$  at mediate times and  $\propto \exp(-t/\tau_{\text{res}})$  at shorter times. It is only in this short time range with exponential decay that the often employed assumption<sup>11</sup> that the ratio  $N_t/n$  is approximately constant is valid. Nevertheless, we find that  $\tau_{\text{res}}$  at high  $G$  is well approximated by  $(1 + N_t/n)\tau_0$ .

The arguments from the related small-signal decay experiment<sup>12</sup> that a high-enough  $G$  has to be employed in order to allow a fast enough emission from the quasi-Fermi-energy also apply here for the validity of the Rose analysis in the large-signal decay, thus for the high- $G$  regime in Fig. 5. The emission time from  $E_{\text{fn}}$  can also be taken as a measure for the time value at which the  $G$  dependence of  $\tau_{\text{res}}$  shows the turnover.

We emphasize that both relations  $\beta = (1 - \gamma)/\alpha$  for low  $G$ , obtained here and by Adriaenssens *et al.* [their Eq. (34)], and also the relation from the Rose analysis  $\beta = 1 - \alpha\gamma$  for high  $G$ , lead to  $\beta = \gamma$  if one assumes  $\gamma = 1/(1 + \alpha)$ . This is confirmed by our numerical modeling in Fig. 5 and the two bottom lines in Table I. Thus with this condition, different values of  $\beta$  and  $\gamma$  for materials like  $a\text{-Si:H}$  or  $a\text{-SiC:H}$  cannot be explained within the often used physical model for amorphous semiconductors with the feature of a single exponential band tail.

We expect the relation for  $\gamma$  to be more complicated, such as just being given by the link to the conduction band tail via  $1/(1 + kT/kT_0)$ . Simulation has shown that the condition for charge neutrality in  $a\text{-Si:H}$  is maintained also by the contribution from charged dangling bonds as well as by the trapped electrons and holes in the conduction and valence band tail.<sup>13,14</sup> Over a larger- $G$  range these simulations show that charge neutrality is maintained by the equality of positive and negative dangling bonds. At higher  $G$  the trapped hole density tracks with the negative dangling bond density and for still higher  $G$  the densities of trapped carriers in the valence and conduction band tail become equal. In contrast, for the validity of  $\gamma = 1/(1 + \alpha)$  the specific equality of the trapped electron density with the density of recombination centers is necessary. Such an equality is not obeyed for the simulation of the photoconductivity of amorphous silicon.<sup>13,14</sup> From temperature-dependent photocurrent experiments on  $a\text{-Si:H}$  and alloys<sup>15</sup> it can be concluded that

$\gamma = 1/(1 + kT/kT_0)$  is only valid in a limited  $T$  range at lower  $T$ . Also, our  $a$ -Si:H samples from plasma-enhanced chemical vapor deposition show  $\gamma$  values at room temperature between 0.8 and 1. Any deduced  $kT_0$  values from these  $\gamma$  values are greater than 100 meV, incompatible with experimental values for the conduction band tail parameter  $kT_0$ .

We have therefore analyzed the relation of  $\gamma$  and  $\beta$  in Fig. 5 and Table I by setting  $\gamma$  independently to 0.8 and 1, values that are found experimentally. In such a case the calculated values for  $\beta$  are much smaller than  $\gamma$ , common to experimental findings summarized in Ref. 1. Having reproduced a general experimental trend, a more detailed comparison with experimental  $\beta$  and  $\gamma$  values requires the identification of the experimental high- or low- $G$  regime with a broader currently not available experimental data base.

There are other amorphous semiconductors like  $a$ -As<sub>2</sub>Se<sub>3</sub> that have been shown to have a featureless exponential band tail.<sup>16</sup> The relations put forward here with the simple physical model can be tested on such a material. Detailed comparison with experimental results from  $a$ -Si:H with its steeper conduction band tail and a dangling bond distribution around midgap can be used to exploit the limits of the model. For this semiconductor the quasi-Fermi-level may be shifted through a nonexponentially varying DOS in the deep band tail or the broad dangling bond distribution.

The existence of the two  $G$  regimes for the decay time in Fig. 5 assists the experimentalist to apply the relation between  $\gamma$  and  $\beta$  for further evaluation. The range of validity

for the determination of a drift mobility,<sup>11</sup> related to the ratio  $N_t/n$  in the high- $G$  regime, can be determined. If  $\alpha$  is to be evaluated one has to make sure which  $G$  regime is probed in the experiment. If a turnover in the  $\tau_{\text{res}}$  value with increasing  $G$  was observed experimentally,  $\alpha$  can be obtained in both regimes and checked for agreement in value and the slope of the DOS distribution can be deduced from the large-signal decay. Finally, our approach may also complement the related analysis of the small-signal decay.<sup>12</sup>

## V. CONCLUSIONS

We developed an approach resulting in closed-form analytical expressions for the decaying electron density based on a rate analysis after termination of steady-state illumination. The improvement in the treatment for the electron decay is evidenced by the agreement with the numerical results. Thereby it is also seen that the TROK model is quite applicable for the photocurrent decay.

Both numerical simulations and our improved analysis show that different values for the exponents  $\beta$  and  $\gamma$  in the generation rate dependence of the response time and the photoconductivity cannot be explained within the applied physical model with a single exponential band tail for amorphous semiconductors, when one assumes the Rose relation  $\gamma = 1/(1 + kT/kT_0)$  to be applicable. The identification of two  $G$  regimes for the dependence of the decay time upon  $G$  by our analysis will assist in the evaluation of experimental data.

\*Present address: Physikalische Chemie, Philipps-Universität Marburg, Hans Meerwein Str., 35032 Marburg, Germany.

†Electronic address: rudi@greco6.physik.uni-oldenburg.de

<sup>1</sup>G. J. Adriaenssens, S. D. Baranovskii, W. Fuhs, J. Jansen, and Ö. Öktü, Phys. Rev. B **51**, 9661 (1995).

<sup>2</sup>G. J. Adriaenssens, S. D. Baranovskii, W. Fuhs, J. Jansen, and Ö. Öktü, J. Non-Cryst. Solids **198-200**, 271 (1996).

<sup>3</sup>A. Rose, *Concepts in Photoconductivity and Allied Problems* (Wiley-Interscience, New York, 1963).

<sup>4</sup>Source available at <http://www.netlib.no/netlib/odepack>, hard-copy documentation in *Scientific Computing*, Vol. 1 of IMACS Transactions on Scientific Computation, edited by R. S. Stepleman *et al.* (North-Holland, Amsterdam, 1983), pp. 55-64.

<sup>5</sup>T. Tiedje and A. Rose, Solid State Commun. **37**, 48 (1981).

<sup>6</sup>J. Orenstein and M. Kastner, Phys. Rev. Lett. **46**, 1421 (1981).

<sup>7</sup>V. I. Arkhipov, M. S. Iovu, A. I. Rudenko, and S. D. Shutov, Phys. Status Solidi **54**, 67 (1979).

<sup>8</sup>R. Brüggemann, Phys. Rev. B **56**, 6408 (1997).

<sup>9</sup>H. Cordes, thesis, Carl von Ossietzky Universität Oldenburg, 1997.

<sup>10</sup>R. H. Bube, *Photoelectronic Properties of Semiconductors* (Cambridge University Press, Cambridge, U.K., 1992).

<sup>11</sup>M. Hoheisel and W. Fuhs, Philos. Mag. B **57**, 411 (1988).

<sup>12</sup>M. Haridim, M. Zelikson, and K. Weiser, Phys. Rev. B **49**, 13 394 (1994).

<sup>13</sup>J. Kočka, C. E. Nebel, and C.-D. Abel, Philos. Mag. B **63**, 221 (1991).

<sup>14</sup>R. Brüggemann, in *Properties of Amorphous Silicon and Its Alloys*, edited by T. M. Searle (Institute of Electrical Engineers, London, U.K., 1998), pp. 217-226.

<sup>15</sup>C.-D. Abel and G. H. Bauer, in *Conference Record 21st IEEE Photovoltaic Specialists Conference, Las Vegas, 1991* (IEEE, New York, 1991), pp. 1550-1554.

<sup>16</sup>D. P. Webb, S. Reynolds, C. Main, Y. C. Chan, Y. W. Lam, and S. K. O'Leary, J. Appl. Phys. **83**, 4782 (1998).